

Atomic-Resolution Imaging of the Nanoscale Origin of Toughness in Rare-Earth Doped SiC

Aaron M. Kueck,^{†,‡} Do Kyung Kim,[§] Quentin M. Ramasse,^{||} L. C. De Jonghe,^{†,‡} and R. O. Ritchie^{*,†,‡}

Materials Sciences Division, and National Center for Electron Microscopy, Lawrence Berkeley National Laboratory, Berkeley, California 94720, Department of Materials Science and Engineering, University of California, Berkeley, California 94720, and Department of Materials Science and Engineering, Korea Advanced Institute of Science and Technology, Daejeon 305–701, Korea

Received June 20, 2008; Revised Manuscript Received July 29, 2008

ABSTRACT

Ultrahigh-resolution transmission electron microscopy and atomic-scale spectroscopy are used to investigate the origin of the toughness in rare-earth doped silicon carbide (RE-SiC) by examining the mechanistic nature of the intergranular cracking events which we find to occur precisely along the RE-decorated interface between the SiC grains and the nanoscale grain-boundary phase. We conclude that, for optimal toughness, the relative elastic modulus across the grain-boundary phase and the interfacial fracture toughness are the most critical material parameters; both can be altered with judicious choice of rare-earth elements.

In brittle materials, fracture toughness is invariably the limiting material property for structural applications; it determines the largest flaw that can be tolerated, which impacts everything from material processing requirements (surface finish, porosity) to strength/fracture loads and fatigue lifetimes.¹ Recent suggestions for improving the toughness of ceramic materials include controlling residual stresses, for example, in glass^{2,3} and alumina,⁴ forming nanocomposites, for example, with carbon nanotubes^{5,6} and nanoceramics,⁷ or using nature-inspired processing.^{8,9} However, the use of sintering additives to create nanometer-scale grain-boundary films or phases has traditionally been the most potent means to develop enhanced toughness in structural ceramics, the objective being to promote intergranular fracture and hence crack deflection and significant crack bridging in the crack wake.

Silicon carbides are potential candidate materials for many ultrahigh-temperature structural applications. For example, using SiC to replace metallic alloys, such as Ni-based superalloys, Ti-6Al-4V, or high-strength steels, in gas-turbine engines for power generation and aerospace applications would permit increases in operating temper-

atures by many hundreds of degrees, with a consequent dramatic increase in thermodynamic efficiency and reduced fuel consumption; however, to date the use of such ceramic materials has been severely limited by their questionable toughness. In light of this, in situ microstructural toughening techniques have been widely attempted to increase the fracture toughness of SiC; using various sintering additives (dopants), the prime objective has been to induce intergranular fracture in order to develop bridging zones in the crack wake from interlocking grains.^{10–13} Intergranular fracture is the essential ingredient here; with a transgranular crack path, no crack bridging can occur with the result that the ceramic has minimal toughness. In addition to the type of dopant, with rare-earth (RE) elements, the presence or absence of intergranular fracture is also related to ionic size.¹⁴ Mechanistically, toughening in liquid-phase-sintered (LPS) materials can be influenced by the mismatch of physical and elastic properties, such as coefficients of thermal expansion (CTE)^{15–17} and elastic constants,^{18,19} between the grain and the grain-boundary phases, which are typically ~ 1 nm in width. In Al₂O₃ and Si₃N₄, CTE mismatch is a source of significant residual stresses, which can lead to enhanced crack deflection and higher toughness. For SiC, conversely, residual stresses are less of a factor as the CTEs of the grains ($\sim 4.5 \times 10^{-6} \text{ }^\circ\text{C}^{-1}$) and boundary phase ($\sim 3\text{--}5 \times 10^{-6} \text{ }^\circ\text{C}^{-1}$)¹⁴ are more comparable. Consequently, toughening is more affected by

* Corresponding author. E-mail: RORitchie@lbl.gov.

[†] Materials Sciences Division, Lawrence Berkeley National Laboratory.

[‡] University of California.

[§] Korea Advanced Institute of Science and Technology.

^{||} National Center for Electron Microscopy, Lawrence Berkeley National Laboratory.

68 the difference in elastic stiffness between the grain and the
69 boundary phase. In situ toughened SiC is therefore an ideal
70 model system for studying the direct role of a nanoscale
71 property, namely, the elastic modulus of the grain-boundary
72 phase, on macroscopic properties such as fracture toughness.

73 To understand the mechanistic processes that induce
74 intergranular fracture in SiC, it is necessary for any crack
75 impinging on a grain boundary not to penetrate that boundary
76 but rather to deflect along the boundary itself. On the basis
77 of crack-deflection mechanics for cracks traversing between
78 elastically dissimilar materials,¹⁸ this would require that
79 intergranular cracks in LPS-SiC ceramics propagate along
80 the grain/boundary-phase interface and not within the phase
81 itself. Although it is the essential precursor to developing
82 any degree of useful toughness in SiC, this critical event
83 has never been experimentally proven. Accordingly, we
84 employ ultrahigh resolution imaging here to reveal the
85 precise, atomistic-scale, nature of the intergranular crack
86 trajectories in SiC with respect to the nanoscale boundary
87 films, using rare-earth additives that segregate to the bound-
88 ary films^{20,21} to decorate the interfaces.

89 Studies were performed on SiC ceramics that were
90 processed with 0.7–1 atom % Y and Yb, as acetate or nitrate
91 salts; the salts were dissolved in methanol and added to
92 submicrometer β -SiC powder (Betarandum, grade Ultrafine,
93 IBIDEN, Japan), with a mean particle size of 0.27 μm , 3 wt
94 % Al metal, 0.6 wt % B, and 6 wt % carbon source. The Al
95 powder (H-3, Valimet, Stockton, CA) had an average size
96 of 3 μm ; the boron powder (Alfa Aesar) had a particle size
97 of less than 5 μm . The carbon was added as polyvinyl-
98 butyral, which yielded $\sim 33\%$ C by weight upon pyrolysis.
99 The powder slurry was ultrasonically agitated, stir-dried, and
100 sieved through a 200 mesh screen. Discs of 38 mm diameter
101 were preformed at room temperature in a steel die, then hot-
102 pressed in a graphite die. Hot pressing was conducted at 1900
103 $^{\circ}\text{C}$ with 50 MPa applied pressure under flowing argon at 1
104 atm, with heating and cooling rates of 10 $^{\circ}\text{C}/\text{min}$.

105 Hot-pressed rounds were ground to remove ~ 0.5 mm from
106 each surface. Transmission electron microscopy (TEM) foils
107 were then prepared from material at least 1 mm from the
108 edge of the specimen. Stable cracks were produced to study
109 the influence of the nanoscale grain-boundary phases on
110 fracture. Cracks in the TEM foils were introduced via
111 indentation, which was performed before final milling on a
112 200 μm thick section; an array of 10 \times 10 microindents (50
113 g load with a cube-corner indenter) was produced on a
114 polished surface. Mechanical thinning and ion milling
115 proceeded from the opposite side to preserve the cracks.
116 Indentation after final milling utilized five indentations, made
117 using a nanoindenter with a corner-cube indenter (under 6000
118 μN normal load), which were placed near the thin edge of
119 the foil to produce cracks which ran toward the thinned
120 region. It was imperative that both crack faces were intact
121 and remained located near each other to allow analysis of
122 mating fracture surfaces. Indentation before or after final foil
123 milling produced identical crack surfaces, indicating that
124 machining and milling during sample preparation had not
125 damaged the crack faces.

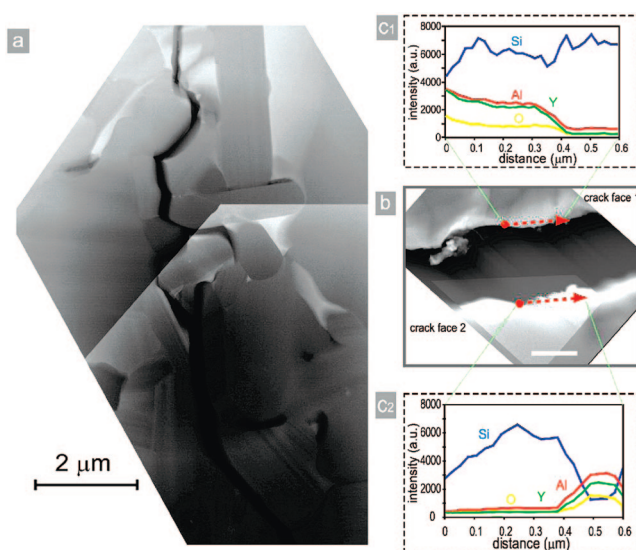


Figure 1. (a) Dark field STEM image of an intergranular crack in SiC with Al, B, C, and Y sintering additives. Crack deflection along grain boundaries is readily apparent; the crack appears black in dark field. (b) Dark field STEM image of two opposing crack faces. Lines along the crack faces indicate the position of EDS line scans, performed with a 1 nm probe size (scale is 500 nm). (c1, c2) Integrated EDS intensity vs distance along the line for Si, Al, Y, and O on each crack face (1 and 2). Grain-boundary phase material (highly enriched in Al, Y, and O) is present along exactly one crack face. This indicates that the fracture location is at the interface between the SiC grain and the grain-boundary phase. Also note that the interface along which the crack propagates switches from crack face 1 (top) to crack face 2 (bottom) near the end of the scan. This could correspond to a change in the direction of the crack.

126 Elemental mapping using electron energy loss spectroscopy (EELS) and nanoprobe energy dispersive spectroscopy (EDS) was conducted using a Philips CM200/FEG STEM. Mapping was performed using a postedge energy-filtered image and background subtraction using two pre-edge images. EDS was carried out in STEM mode with a 1 nm spot size. Signals were integrated over the peak width using the Si, Al, and O K-lines and either the RE K- or L-lines. High-resolution high-angle annular dark field (HAADF) images and EELS were performed using a VG HB501 dedicated STEM with a spot size of 1 \AA (imaging) or 1.5 \AA (spectroscopy). Semiconvergence angles were 20 mrad (imaging) and 28 mrad (spectroscopy). The HAADF collection angle range was 74–215 mrad; the EELS collection angle was 12 mrad, and the resolution was 0.1 eV. Spectroscopic methods were used to determine the relative location of the crack paths with respect to the SiC grains and the nanometer-wide grain-boundary phases.

144 EDS line scans of opposing crack faces (Figure 1) and
145 elemental mapping with EELS (Figure 2) both demonstrated
146 that the intergranular cracks formed along the nanometer-
147 wide grain-boundary phase (GBP). Segregation of Al, O, and
148 RE could be clearly identified in this phase, with the cracks
149 located strictly along one side of the boundary phase. Figure
150 1c highlights the contrast between the compositions of the
151 two crack faces. While one fracture surface exhibits Al, Y,

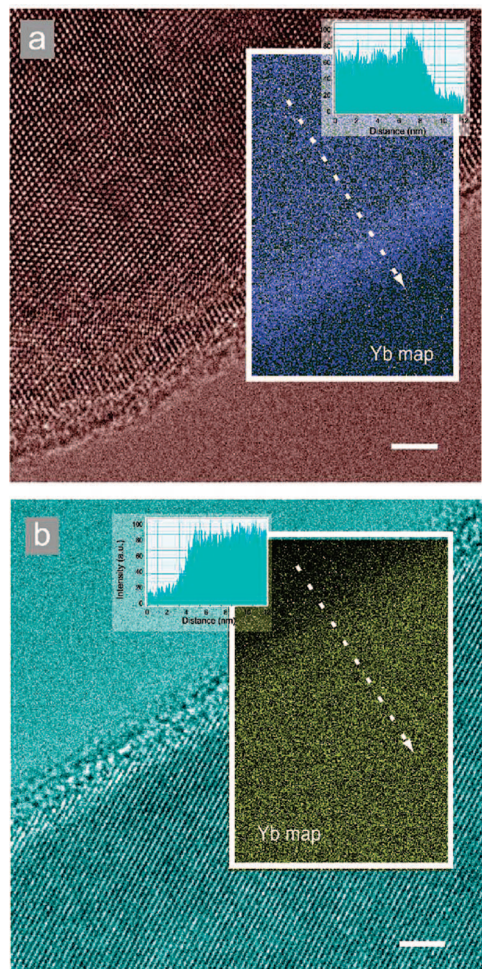


Figure 2. (a) Bright field HRTEM and Yb elemental map (overlay) of an intergranular crack face in SiC with Al, B, C, and Yb additives (scale is 2 nm). The Yb map shows a dramatic increase in the Yb signal along the edge of the crack (see intensity profile inset), indicating the presence of the grain-boundary phase. Nanoprobe EDS at the edge confirms enrichment of Yb, Al, and O. (b) Bright field HRTEM and Yb elemental map (overlay) of the intergranular crack face opposite that in Figure 2a. The Yb map shows no contrast (see intensity profile inset), indicating the lack of Yb along this crack face. Nanoprobe EDS at the edge finds (1) bulk value of Al, (2) lack of Yb, and (3) slight enrichment of O. This indicates that the crack propagates precisely along the interface between the SiC grain and the RE-bearing grain-boundary phase, as is seen in the material with Y (Figure 1).

152 and O signals that approach or exceed Si, the opposite surface
 153 contains only background counts of the GBP constituents.
 154 Figure 2 shows this contrast visually; the bright edge along
 155 one fracture surface reveals the Yb present only in the
 156 boundary phase. Indeed, all intergranular cracks in both Y-
 157 and Yb-containing materials showed identical behavior with
 158 the intergranular crack following an exact path along one
 159 side of the boundary phase.

160 The side of the crack not adjacent to grain-boundary
 161 material was chemically indistinguishable from the center
 162 of a SiC grain. The crack surface on this side was slightly
 163 enriched with oxygen (O), although high-spatial-resolution
 164 EELS suggested that minimal O enrichment is a characteristic
 165 of the SiC lattice near grain boundaries. Figure 3 shows that

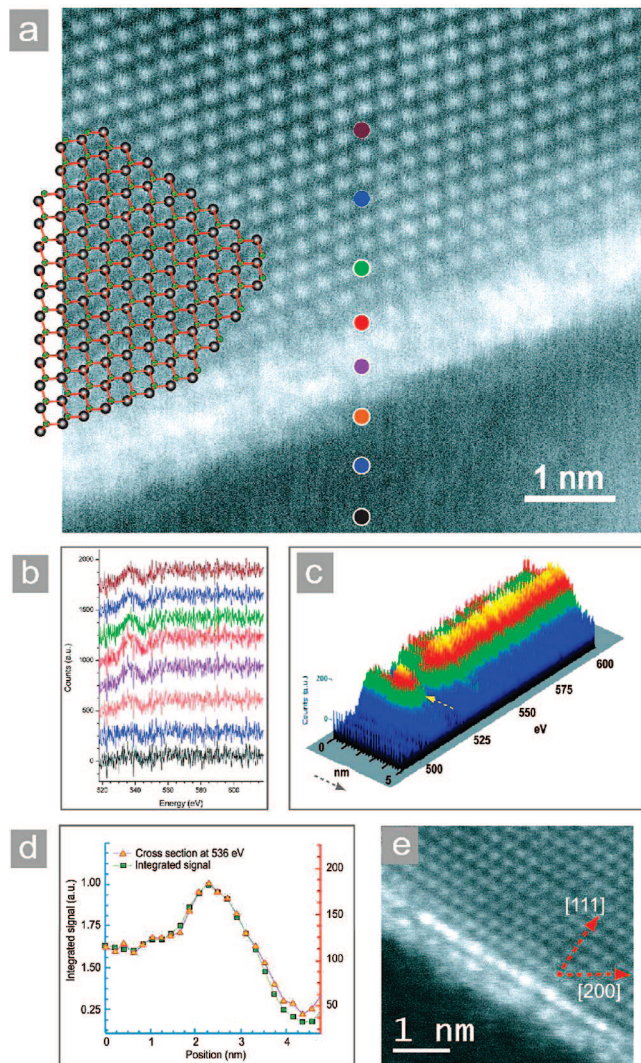


Figure 3. (a) Z-contrast image of a grain boundary. Bright contrast in the grain-boundary phase indicates enrichment of Yb. (b) O K-edge EELS scans along the line indicated in Figure 3a. O peak height is greatest within the grain-boundary phase. (c) 3-D plot of the EELS scans along the line in Figure 3a. The O peak is indicated with an arrow. The O chemical width of the boundary is ~ 2 nm; this is twice the Yb chemical width from the Z-contrast image. Crack propagation occurs along the interface determined by the enrichment of RE, not the interface determined by O. This is a sensible result as RE-C(O) bonds should be weaker than Si-C(O) bonds; the RE-containing interface is the weakest plane and most likely to fracture. (d) O peak height at 536 eV and total O peak integrated intensity from 528 to 624 eV vs distance along the scan. The chemical width of the grain-boundary phase is ~ 1.4 nm, and there is an area of O enrichment ~ 1 nm in width in the aligned grain (upper portion of 3a). (e) Yb-enriched grain boundary which has been aligned with the beam to show the location of the RE columns. Yb-containing columns terminate each plane of the SiC lattice, aligning along the [200] direction.

166 the O peak height near a grain boundary is increased ~ 1
 167 nm into the SiC grain, well beyond the extent of the GBP.
 168 Indeed, enrichment of O near grain boundaries has been
 169 predicted in silicon nitride, which has similar grain-boundary
 170 phases.^{22,23} Our analysis of numerous similar foils confirmed
 171 that this specific location of the fracture was definitively
 172 between the RE-containing grain-boundary phase and the

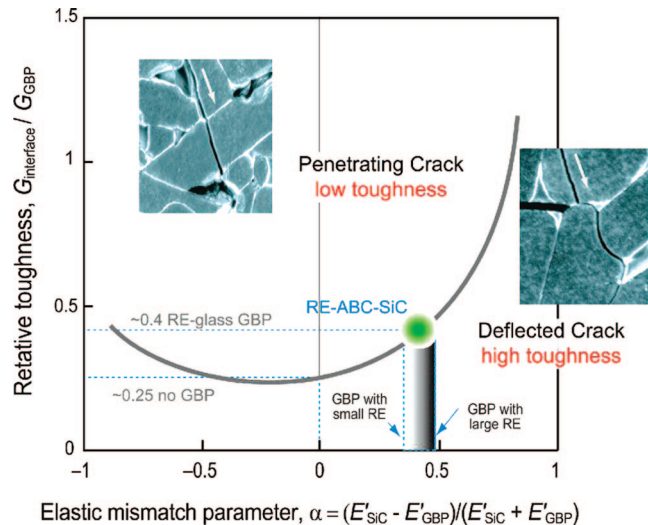
173 O-enriched SiC lattice, which strongly implies that the
 174 interface defined by RE segregation is the most relevant for
 175 fracture. This points to the plane containing RE-C(O) bonds
 176 as the weakest link, making this interface the most likely to
 177 fracture.

178 Figure 3e shows a Yb-enriched grain boundary which has
 179 been aligned with the beam to show the location of RE-
 180 containing columns along the interface. Bright columns,
 181 indicating the presence of RE atoms, can be seen to terminate
 182 each SiC plane along the [200] direction. Unlike Si₃N₄, which
 183 often exhibits two possible RE locations along the inter-
 184 face,^{21,22} the GBP in SiC has only one interfacial RE location.
 185 This coincides with the difference in the structure of the
 186 ceramic surfaces. Si₃N₄ interfaces consist of open rings,
 187 leading to two possible attachment locations, whereas SiC
 188 interfaces are atomically flatter, presenting only one possible
 189 attachment location for the large RE atoms.

190 This result, that any crack impinging on the grain-boundary
 191 phase will not penetrate the phase but rather “delaminate”
 192 along the boundary-phase/SiC interface, is entirely consistent
 193 with linear-elastic crack deflection mechanics, specifically
 194 the He and Hutchinson solution¹⁸ for predicting whether a
 195 crack penetrates or arrests/delaminates at a dissimilar material
 196 interface. The important parameters in this model are (i) the
 197 incident angle, which is microstructure-dependent, (ii) the
 198 modulus mismatch across the interface $(E'_{SiC} - E'_{GBP}) / (E'_{SiC} + E'_{GBP})$, that is, the relative elastic modulus of the boundary
 199 phase, which is chemistry- and structure-dependent (E'_{SiC} and
 200 E'_{GBP} are, respectively, the Young’s moduli of the SiC grain
 201 and boundary phase), and (iii) the relative fracture toughness
 202 of the interface $G_{interface}$ (which depends on the interface
 203 bonding) and that of the boundary phase G_{GBP} . Rare-earth
 204 additives can alter both the stiffness of the boundary phase
 205 and the toughness of the interface.

207 Figure 4 presents the He and Hutchinson solution for SiC/
 208 GBP with a crack at an interface incident at 90°, showing a
 209 plot of the relative interfacial toughness versus the relative
 210 elastic modulus along with a bounding line between interface
 211 penetration or deflection (interface delamination). Normal
 212 incidence along the boundary represents the geometrically
 213 worst-case scenario; a shallower angle increases the likeli-
 214 hood for crack deflection. Included are images of cracks in
 215 RE-doped SiC at near 90° incidence. The observation of both
 216 crack penetration and deflection suggests that the RE-SiC
 217 system is near the bounding line between these two types of
 218 cracking behavior and is therefore very sensitive to the choice
 219 of rare-earth dopant. This presents the opportunity to estimate
 220 the relative interfacial toughness in our system, if the elastic
 221 properties of the boundary phase are known.

222 Possible values for the elastic modulus of the GBP vary.
 223 Oxynitride glasses have low elastic moduli, with $E \sim 150$
 224 GPa.²⁴ Crystalline Al₂O₃, a second phase material commonly
 225 seen in ABC-SiC and a possible GBP, has a much higher E
 226 of 225 GPa.²⁵ An intermediate modulus of 209 GPa has been
 227 calculated for the GBP of Si₃N₄ with Y.²⁶ Using this latter
 228 value of E for the GBP, we can estimate the relative
 229 interfacial toughness in our material as 0.4 times the
 230 toughness of the GBP.



231 **Figure 4.** He and Hutchinson’s solution for a crack impinging an
 232 interface between two elastically dissimilar materials at 90°. The
 233 curve marks the boundary between systems in which cracks are
 234 likely to penetrate the interface (above the curve) or deflect
 235 along the interface (below the curve). Experimental trends in RE-doped
 236 SiC show a transition from crack deflection to interface penetration
 237 as the radius of the RE ion decreases, suggesting that these systems
 238 lie near the bounding curve. Shown are likely values for the elastic
 239 mismatch, based on calculated elastic modulus values for the
 240 boundary phase (E_{GBP}).²⁶ The interfacial toughness is then ~ 0.4
 241 times the toughness of the grain-boundary phase. Small deviations
 242 in interfacial toughness, driven by changes in the ionic size of the
 243 RE additives along the interface, can push the crack to deflect along
 244 the boundary (large RE), resulting in intergranular fracture and high
 245 toughness, or penetrate the boundary (small RE), resulting in
 246 transgranular fracture and minimal toughness.

231 On the basis of bulk glass measurements and simulations
 232 of the properties of the grain-boundary phases, it is expected
 233 that the addition of RE will increase the modulus of the grain-
 234 boundary phase,^{26,27} with smaller ions having the larger
 235 effect. With a larger E'_{GBP} associated with the addition of
 236 RE ions, the elastic mismatch between SiC and the boundary
 237 phase will be progressively decreased, which from Figure 3
 238 will reduce the likelihood of crack deflection along, rather
 239 than through, the interface. This implies that the addition of
 240 smaller RE ions to SiC should diminish the probability of
 241 intergranular fracture and hence degrade the toughness, as
 242 has been seen experimentally.^{14,28,29}

243 RE additives should also affect the toughness of the
 244 interface. RE ions can act as network modifiers in glassy-
 245 boundary phases; high-coordination, large radius RE ions
 246 should lower the local strength of the glass.³⁰ Replacing a
 247 Si or Al atom along the interface with a RE ion would be
 248 expected to lower the toughness of the interface;^{31,32} accord-
 249 ingly, large RE ions will certainly have the greatest effect.
 250 The largest decrease in interfacial toughness in the presence
 251 of large RE ions, combined with a lower elastic modulus of
 252 the boundary phase, makes crack deflection at, and then
 253 “delamination” along, the interface more likely; this confirms
 254 that doping with large RE ions will promote intergranular
 255 fracture and hence enhance the toughness of the ceramic,
 256 again consistent with experiments.^{14,28,29}

257 In conclusion, nanoscale-resolution microscopy and spec-
 258 troscopy has demonstrated that intergranular cracks in SiC
 259 with rare-earth additives propagate precisely along the
 260 interface between the SiC grains and the nanometer-wide
 261 RE-containing grain-boundary phase. This fracture behavior
 262 can be understood in terms of the He and Hutchinson model
 263 for the interaction of elastic cracks with interfaces. Crack
 264 deflection along the interface in these materials can be altered
 265 by choice of rare-earth elements; larger ions enhance the
 266 likelihood of intergranular fracture and consequently increase
 267 the toughness, providing a striking example of the direct link
 268 across some eight orders of dimensions between nanoscale
 269 events and the macroscopic mechanical properties of materi-
 270 als.

271 **Acknowledgment.** This work was supported by the
 272 Director, Office of Science, Office of Basic Energy Sciences,
 273 Materials Sciences and Engineering Division, of the U.S.
 274 Department of Energy under Contract No. DE-AC02-
 275 05CH11231. Part of this work was carried out using the
 276 facilities at the National Center for Electron Microscopy,
 277 which is supported at the Lawrence Berkeley National
 278 Laboratory by the Department of Energy under the same
 279 contract number. D.K.K. would like to thank the SBS
 280 Foundation for supporting his sabbatical leave in Berkeley
 281 where the study was performed.

282 References

- 283 (1) Clegg, W. J. *Science* **1999**, 286, 1097–1099.
 284 (2) Green, D. J.; Tandon, R.; Sglavo, V. M. *Science* **1999**, 283, 1295–
 285 1297.
 286 (3) Zhang, Y.; Wang, W. H.; Greer, A. L. *Nat. Mater.* **2006**, 5, 857–860.
 287 (4) Rao, M. P.; Sanchez-Herencia, A. J.; Beltz, G. E.; McMeeking, R. M.;
 288 Lange, F. F. *Science* **1999**, 286, 102–105.
 289 (5) Zhan, G.-D.; Kuntz, J. D.; Wan, J.; Mukherjee, A. K. *Nat. Mater.*
 290 **2002**, 2, 38–42.
 291 (6) Peigney, A. *Nat. Mater.* **2002**, 2, 15–16.
 292 (7) Zhang, X. F.; Harley, G.; De Jonghe, L. C. *Nano Lett.* **2005**, 5, 1035–
 293 1037.

- (8) Deville, S.; Saiz, E.; Nalla, R. K.; Tomsia, A. P. *Science* **2006**, 311, 294
 515–518. 295
 (9) Ahn, E. S.; Gleason, N. J.; Nakahira, A.; Ying, J. Y. *Nano Lett.* **2001**, 296
 1, 149–153. 297
 (10) Cao, J. J.; MoberlyChan, W. J.; De Jonghe, L. C.; Gilbert, C. J.; 298
 Ritchie, R. O. *J. Am. Ceram. Soc.* **1996**, 79, 461–469. 299
 (11) Zhang, X.-F.; Yang, Q.; De Jonghe, L. C. *Acta Mater.* **2003**, 51, 3849– 300
 3860. 301
 (12) Lee, S.; Kim, Y.; Mitomo, M. *J. Am. Ceram. Soc.* **2001**, 84, 1347– 302
 1353. 303
 (13) Strecker, K.; Ribeiro, S.; Oberacker, R.; Hoffmann, M.-J. *Int. J.* 304
Refract. Metals Hard Mat. **2004**, 22, 169–175. 305
 (14) Zhou, Y.; Hirao, K.; Toriyama, M.; Yamauchi, Y.; Kanzaki, S. *J. Am.* 306
Ceram. Soc. **2001**, 84, 1642–1644. 307
 (15) Hsueh, C.-H.; Becher, P. F. *Mater. Sci. Eng., A* **1996**, 212, 22–28. 308
 (16) Li, Z.; Bradt, R. C. *J. Am. Ceram. Soc.* **1989**, 72, 70–77. 309
 (17) Peterson, I. M.; Tien, T.-Y. *J. Am. Ceram. Soc.* **1995**, 78, 2345–2352. 310
 (18) He, M.-Y.; Hutchinson, J. W. *Int. J. Solids Structures* **1989**, 25, 1053– 311
 1067. 312
 (19) McNaney, J. M.; Cannon, R. M.; Ritchie, R. O. *Int. J. Fract.* **1994**, 313
 66, 227–240. 314
 (20) Ziegler, A.; Idrobo, J. C.; Cinibulk, M. K.; Kisielowski, C.; Browning, 315
 N. D.; Ritchie, R. O. *Science* **2004**, 306, 1768–1770. 316
 (21) Dwyer, C.; et al. *J. Mater. Sci.* **2006**, 41, 4405–4412. 317
 (22) Bishop, C. M.; Cannon, R. M.; Carter, W. C. *Acta Mater.* **2005**, 53, 318
 4755–4764. 319
 (23) Hudson, T. S.; Nguyen-Mahn, D.; van Duin, A. C. T.; Sutton, A. P. 320
Mater. Sci. Eng., A **2006**, 422, 123–135. 321
 (24) Becher, P. F.; et al. *Acta Mater.* **1996**, 44, 3881–3893. 322
 (25) Yu, R.; Zhang, X.-F.; De Jonghe, L. C.; Ritchie, R. O. *Phys. Rev. B* 323
2007, 75, 104114. 324
 (26) Chen, J.; Ouyang, L.; Rulis, P.; Misra, A.; Ching, W. Y. *Phys. Rev.* 325
Lett. **2005**, 95, 256103. 326
 (27) Hampshire, S.; Pomeroy, M. J. *J. Non-Cryst. Solids* **2004**, 344, 1–7. 327
 (28) Satet, R. L.; Hoffmann, M. J.; Cannon, R. M. *Mater. Sci. Eng., A* 328
2006, 422, 66–76. 329
 (29) Liu, Q.; Gao, L.; Yan, D. S.; Thompson, D. P. *Mater. Sci. Eng., A* 330
1999, 269, 1–7. 331
 (30) Marchi, J.; Morais, D. S.; Schneider, J.; Bressiani, J. C.; Bressiani, 332
 A. H. A. *J. Non-Cryst. Solids* **2005**, 351, 863–868. 333
 (31) Nakayasu, T.; Yamada, T.; Tanaka, I.; Adachi, H.; Goto, S. *J. Am.* 334
Ceram. Soc. **1998**, 81, 565–570. 335
 (32) Sun, E. Y.; Alexander, K. B.; Becher, P. F.; Hwang, S.-L. *J. Am.* 336
Ceram. Soc. **1996**, 79, 2626–2632. 337

NL8017884

338